Spectral Manipulation of Raman Amplifiers

IOP Conf. Series: Journal of Physics: Conf. Series **1206** (2019) 012015 doi:10.1088/1742-6596/1206/1/012015

Spectral Manipulation of Raman Amplifiers

I Barth[1] **and N J Fisch**[2]

[1] Racah Institute of Physics, Hebrew University of Jerusalem, 91904, Jerusalem, Israel.
Contact Phone: +972524474611
[2] Department of Astrophysical Sciences, Princeton University, 08544, Princeton NJ, USA

E-mail: ido.barth@mail.huji.ac.il

Abstract. Backward Raman amplifiers provide a promising path to the next generation of short pulse high-intensity lasers that can go beyond the damage limit of conventional materials. The main idea is to couple a short seed and a long counter-propagating pump through an electron plasma wave in such a way that the pump energy is transferred to the seed that is amplified and compressed via Raman backscattering. This paper will shortly review the physics of Raman amplifiers including two recent developments in the field: (a) mitigating the relativistic phase-mismatch and the resulting saturation by detuning of the pump pulse and (b) multi-frequency amplification of pulses with a beat-wave waveform.

1. Introduction

1.1. Overview

One of the most promising paths to the next generation of short pulse ultra-high intensity lasers are the backward Raman amplifiers (BRA) that enjoy the property of circumventing the damage limit of conventional solid-state devices. The main idea is to use plasmas as the amplifying media. In particular, one would want to couple a short seed and a long counter-propagating pump through a plasma wave in such a way that the pump energy is transferred to the seed that, in turn, is amplified and compressed via parametric backscattering [1]. The two main parametric processes are the stimulated Raman backscattering (SRS) and the stimulated Brillouin backscattering (SBS). The mediating plasma waves are electron plasma wave (EPW) for SRS and ion acoustic wave for SBS [2, 3]. We will focus here on BRA since they enjoy a larger growth rate although Brillouin amplifiers could, in principle, be advantageous in some regimes [4].

The amplification dynamics comprises two successive stages. The first stage is the linear regime in which the short seed grows exponentially while the pump pulse remains approximately unchanged. The seed growth is accompanied by exponentially growing EPW that serves as the energy mediator in the well know Raman three-wave interaction. At this stage, the linear growth rate for linearly polarized pulses can be approximated by $\Gamma \approx a_0\sqrt{\omega_a\omega_e}/2$, where a_0 is the dimensionless pump amplitude and $\omega_{a,e}$ are the pump and plasma frequencies, respectively. After a few e-foldings, when the amplitudes of the amplified seed pulse and of the EPW become sufficiently large, the pump pulse depletes a significant amount of its energy so it cannot be treated as a constant. This second stage is called the pump depletion regime or the nonlinear regime since all of the three waves change in time and the three-wave-interaction model becomes

nonlinear. In this regime, the depleted pump energy is distributed between the amplified seed and the EPW according to the Manley-Rowe relations.

1.2. The fluid model

The simplest way to model the system is by the envelope-approximated fluid model [1] that describes the dynamics of the envelopes of the waves while assuming a single carrier frequency for each wave. Moreover, this model also considers perfect spacial and temporal resonance conditions,

$$\omega_a = \omega_b + \omega_e \tag{1}$$
$$k_a = k_b + k_f \tag{2}$$

where, for Raman backscattering the pump pulse and the EPW wave vectors, k_a and k_f, respectively, have the same sign while the sign of seed wave vector, k_b is opposite. This reflects the fact that the seed and the pump pulses are counter-propagating. The temporal resonance condition implies that when preparing the system, one must ensure that the seed frequency, ω_b is downshifted with respect to the pump frequency, ω_a by the plasma frequency, ω_e. It is noted that Brillouin amplifiers do not require such a condition since the frequency of the ion acoustic wave is negligible compared to those of the electromagnetic waves. It is also importantly noted that this requirement can be waived by using plasma-wave seed instead of laser seed [5]. However, in this paper, we focus on the traditional setup with a laser seed.

The envelope-approximated fluid model for BRA is given by the three-wave interaction equations,

$$a_t + c_a a_z = V_3 f b \tag{3}$$
$$b_t - c_b b_z = -V_3 a f^* \tag{4}$$
$$f_t = -V_3 a b^* \tag{5}$$

where, the pump and seed group velocities are $c_{a,b} = c\sqrt{1-\omega_e^2/\omega_{a,b}^2}$, c being the speed of light. For linear polarizations, the three-wave coupling coefficient is given by $V_3 \approx \sqrt{\omega_e \omega_a}/2$ that is related to the linear growth rate via $\Gamma \approx a_0 V_3$. The amplified pulse intensity scales as $I \sim b^2$.

It is critical that, under certain conditions, the three wave interaction system can be reduced to the well known Sine-Gordon equation [1]. A self-similar solution that was found via the inverse scattering transform describing a kink-like solution of the amplified seed pulse rads,

$$b \sim \frac{2\tau}{(\xi+1)\cosh(\xi-\xi_M)}. \tag{6}$$

Here, $\tau \sim (L-z)/c$ is the dimensionless amplification time, $\zeta \sim t-(L-z)/c$ is the dimensionless delay time and $\xi = 2\sqrt{\tau\zeta}$ is an auxiliary variable for the sine-Gordon equation $u_{\zeta\tau} = \sin u$ (for more details see Ref. [6] and the appendix therein). This analytical solution provides a solid base for the inclusion of higher order physical effects by the means of perturbation theories. The main outcome of this analytical solution is that in the nonlinear regime the peak intensity scales as $I_{\max} \sim b_{\max}^2 \sim \tau^2$ while its width scales as $\Delta I \sim \tau^{-1}$ so the total fluence, $W = \int I d\zeta$, grows linearly with τ.

1.3. Typical parameters

Although multiple parameter regimes were studied for BRA [7], let us consider one typical set of parameters. Such an example is presented in Table 1. The three most important parameters

Table 1. A typical set of parameters for Raman amplifiers.

Parameter	Symbol	Value	Units
Pump wavelength	λ_a	1	μm
Pump frequency	ω_a	300	$2\pi \times$ THz
Electron density	n_e	10^{19}	cm^{-3}
Plasma frequency	ω_e	28	$2\pi \times$ THz
Plasma length	L	1	cm
Pump intensity	I_a	10^{14}	$\mathrm{W/cm}^2$
Dimensionless amplitude	a_0	0.008	—
Amplified intensity	$I_b^{\max}$	10^{17}	$\mathrm{W/cm}^2$
Raman growth rate	Γ	2	ps^{-1}
Frequencies ratio	q	0.1	—

are the pump wavelength, λ_a, the plasma density, n_e, and the dimensionless pump amplitude, a_0. The first two parameters determine the ratio between the plasma and the pump frequencies,

$$q = \frac{\omega_e}{\omega_b}, \tag{7}$$

which is the main parameter in determining the properties of various physical effect in Raman amplifiers. For the example presented in Table 1 we have the typical value of $q \approx 0.1$. This means that the considered plasma is quite underdence, $n_e \approx 0.01 n_{cr}$, where $n_{\mathrm{cr}} = 1.1 \times 10^{21} (\lambda_a[\mu m])^{-2}\,\mathrm{cm}^{-3}$ is the critical density, and the seed frequency is downshifted by about 10 percent from the pump laser to fulfil the resonance condition in Eq. (1). The next subsection discusses a few of these effects.

1.4. Limitations

Generally speaking, BRA is applicable and efficient for a finite parameter space. First, due to the frequency downshifting of the backscattered light, Raman backscattering occurs only for plasma densities below one-quarter the critical density, $n_e < 0.25\, n_{\mathrm{cr}}$.

The second and maybe the most challenging limitation is the transverse modulation instabilities. When the laser power becomes sufficiently large, the plasma behaves as a focusing Kerr medium and the amplified pulse breaks into transverse filaments. The criterion for the laser power, P, to avoid plasma heating that results in modulation instability is $P < P_{\mathrm{cr}} \approx 17/q^2\,\mathrm{GW}$. To extend the amplification lengths, it was recently suggested to use random fluctuations of the refractive index in order to overcome this instability [19]. The physical mechanisms underlying this suggestion are much like for random phase plates, only here the randomization occurs over a volume. In this case, the focusing would have to be accomplished in a second stage.

There are two more kinetic effects that limit the BRA efficiency: wave breaking and Landau damping. First, to avoid wave breaking of the EPW, the (dimensionless) pump amplitude, a_0, must obey $a_0 \le a_{\mathrm{wb}} = 0.25\, q^{3/2}$. Note that for the typical example of Table 1 we have $a_{\mathrm{wb}} = 0.008$ so a_0 is just before the wave breaking regime. The other kinetic limitation requires sufficiently cold plasma, $T_e \ll T_M \approx 127\, q^2$ KeV (T_e is the electron temperature) to avoid Landau damping.

2. Nonlinear saturation and beyond

2.1. Nonlinear saturation

While the approximated fluid model (3-5) was quite useful for getting an analytical solution that elucidates the dynamics of BRA, it neglects several effects. One of these is the relativistic motion of the electrons when the electric field of the amplified pulse becomes sufficiently large. For weakly relativistic nonlinearity, this effect can be taken into account within the fluid model by adding a cubic term to Eq. (4) [8]. It is sufficient to modify only the equation for the amplified pulse amplitude, since the pump amplitude, a, is bounded by a_0, which is not so large as to incur relativistic effects, while the amplified pulse amplitude, b, is amplified to intensities large enough to encounter these relativistic effects. The revised fluid model reads

$$\begin{aligned} a_t + c_a a_z &= V_3 f b & (8)\\ b_t - c_b b_z &= -V_3 a f^* + iR|b|^2 b & (9)\\ f_t &= -V_3 a b^* & (10) \end{aligned}$$

where $R \approx \omega_e^2/8\omega_b$. It was found in Ref. [8] that the relativistic motion of the electrons results in a saturation of the leading spike of the amplified pulse. Moreover, it was found that after the saturation of the leading spike, a secondary spike gets amplified and after its saturation, a third spike appears in turn [9]. The resulting amplified pulse is then, a multispike pulse, where the maximal intensity is accepted in a secondary spike rather than in the leading spike as desire.

In order to overcome this nonlinear saturation we first identified that the reason for the saturation is the phase mismatch accumulation that is associated with the imaginary term $iR|b|^2 b$ as follows. We define the phases of the pump, seed, and plasma waves by ϕ_a, ϕ_b, and ϕ_f, respectively, where for perfect resonance conditions (1,2), the total phase mismatch, $\Phi = \phi_a - \phi_b - \phi_f$, vanishes. Notably, the zero-order analytical solution [Eq. (6)] can be employed to estimate the evolution of this phase mismatch. After some algebra, the solution for the phase mismatch at the leading peak of the amplified pulse reads $\Phi + \frac{1}{3}\Phi^3 + \mu = 0$, where, $\mu = \frac{4\tau^3}{3(\zeta_M+1)^2}$ and ζ_M is a dimensionless parameter, which is determined by the initial conditions [6]. The real solution for Φ is then

$$\Phi = \eta^{\frac{1}{3}} - \eta^{-\frac{1}{3}}, \qquad (11)$$

where $\eta = -\frac{3\mu}{2} + \sqrt{1 + \frac{9\mu^2}{4}}$. It is notable that for a given amplification time τ, this solution depends on one parameter only, ξ_M. For the example presented in Fig. 1, we have $\epsilon = 0.1$ so $\xi_M = 5.5$. In the upper panel of the figure, we plot the analytical solution (6) for the maximal amplitude of the leading spike, $B_{\max}(\tau)$, (black line with squares). In the lower panel of the figure, we compare our theoretical prediction (11) for the phase mismatch of the leading spike, Φ, (black line with squares) with the simulation results (blue dashed-dotted line). It is notable, that the theory, which does not contain any adjustable parameter, is in a high agreement with the numerical solution.

2.2. Pump detuning

After we have identified the source of the saturation, the way to overcome this saturation is clear. The phase mismatch causing the saturation should be compensated by an external detuning. In principle, there are two phases that we can detune in order to maintain the phase-locking: the laser pump pulse and/or the electron plasma wave, where the latter is realized by a density gradient. However, since $\omega_p \ll \omega_a$, the contribution of density gradients to the overall phase compensation is quite modest. According to the analytical solution for the phase-mismatch of the leading spike, Φ, [Eq. (11)] we choose to detune the pump frequency as a power law in the amplification time,

$$\delta\omega \sim \tau^\gamma. \qquad (12)$$

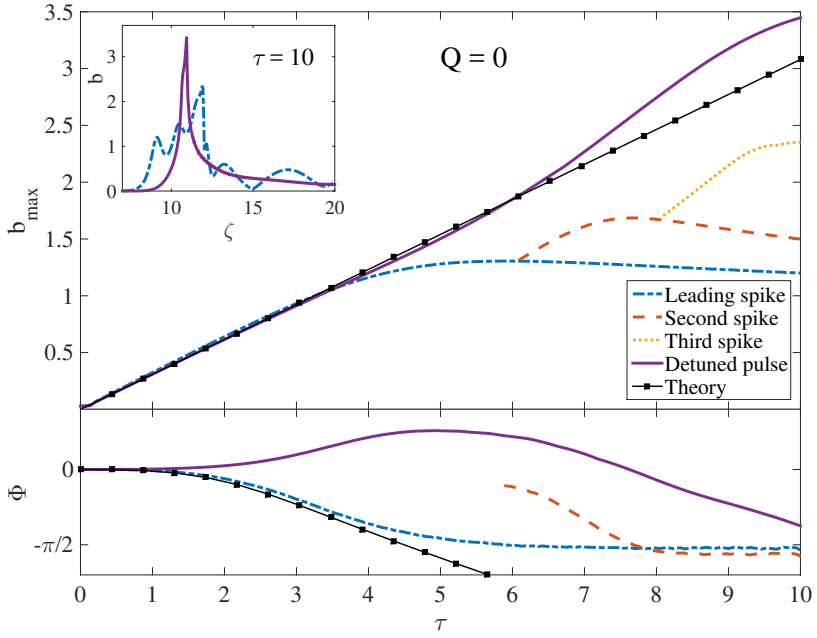

Figure 1. (Taken from Ref. [6]). The maximal amplitude, $b_{\max}$, (upper panel) and the phase mismatch, Φ, (lower panel) of the amplified pulse as a function of the amplification time, τ, in the dispersionless ($Q = 0$) regime. $b_{\max}$ and Φ of the leading (dashed-dotted), second (dashed) and third (dotted) spikes of the saturated unchirped ($\Delta = 0$) pulse are compared with those of the detuned pulse (solid line) and with the theoretical predictions (solid lines with squares), for $b_{\max}$ for Φ. The final $\tau = 10$ profiles of the singled-spike detuned (solid) and of the multi-spike undetuned (dashed-doted) are compared in the inset.

In order to illustrate the effect of chirping we used $\gamma = 4$ in the example in Fig. 1. As shown in the figure, the advantage of the chirped pump is twofold. First, the seed amplification is enhanced beyond the nonlinear saturation limit, where the peak intensity is more than as twice as the unchirped case. Second, the amplified pulse is reshaped into a single spike pulse as shown in the inset of Fig. 1. As a result, most of the power resides in the leading spike with less precursory power ahead of it so the leading spike intensity is enhanced by a factor of 6.

In addition, we have scanned the parameter space in order to draw a roadmap for the optimization of the amplification enhancement. This roadmap is presented and discussed in Ref. [6]. The main result is the existence of a threshold for the amplification enhancement, in which, too fast chirps break the Raman resonance condition at early times so the overall amplification is poor. Notably, this effect is important for noise suppression [10]. On the other hand, too slow chirps cannot compensate the phase mismatch accumulation at later times resulting in an ineffective amplification enhancement but no sharp threshold was observed.

2.3. The effect of group velocity dispersion

The promising results of the previous section were based on the dispersionless fluid model. However, when considering a more realistic model that includes also the group velocity dispersion (GVD) of the amplified pulse the enhancement effect becomes more modest. GVD can be included in the fluid model by introducing a term in the right-hand side of Eq. (9) so it reads

$$b_t - c_b\, b_z = -V_3\, a\, f^* + iR|b|^2 b - i\kappa b_{tt}. \tag{13}$$

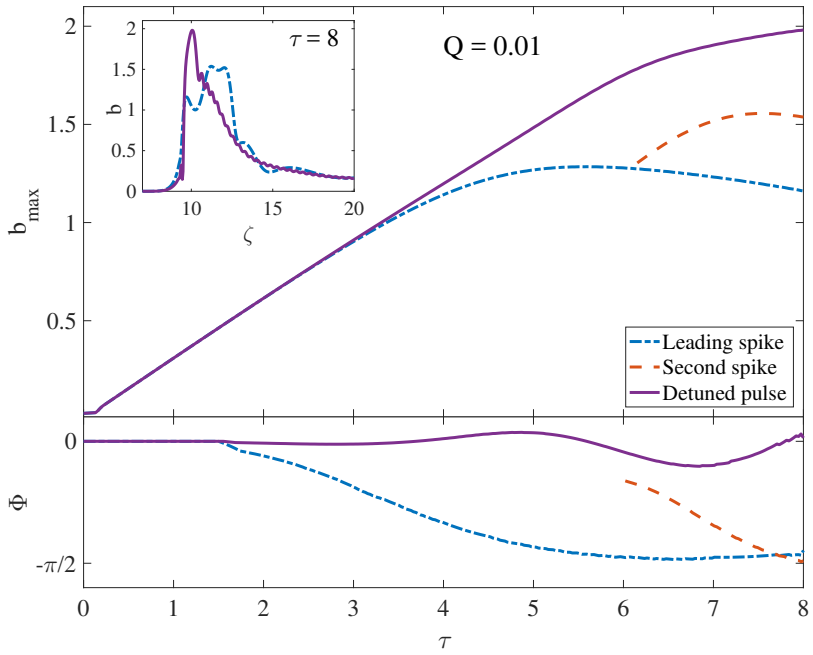

Figure 2. (Taken from Ref. [6]). Similar to Fig 2.1 but for a dispersive model with a finite GVD coefficient, $Q = 0.01$.

Here, the GVD coefficient is $\kappa = \frac{1}{2c_b}\frac{dc_b}{d\omega} \sim Q^2$ and $Q = \frac{\omega_e}{2\omega_b} \approx q/2$. An example of a chirped amplifier with finite GVD of $Q = 0.01$ is presented in Fig. 2. The example in the figure shows that a more realistic model that includes GVD has a reduced amplification enhancement but smoother spikes. A more comprehensive discussion on the optimization of the amplification enhancement in the GVD regime can be also found in Ref. [6].

3. Multifrequency amplification

In the previous section, we have shown how spectral manipulation (i.e., pump detuning) can enhance the Raman amplification and improve the amplified pulse shape. However, the pump and seed comprise only one carrier frequency. Remarkably, this is usually considered for both Raman and Brillouin amplifier. A question that may be asked is whether we can Raman-amplify a pulse with more than one carrier frequency?

Next, we show that, indeed, a wave packet comprising two or more well-separated carrier frequencies can be amplified with a similar efficiency as a single-frequency pulse even in the nonlinear regime. We call this regime multifrequency BRA (MFBRA) to distinguish it from the usual single frequency BRA (SFBRA). Importantly, in addition to mitigating the premature backscattering of the multifrequency pump [11] that is common to other methods that require bandwidth [12, 13, 14], MFBRA is advantageous because of its beat-wave waveform. In such a waveform, the width of each spike is smaller than the whole pulse envelope width, a feature that can be used advantageously. Moreover, we found that by a proper preparation of the initial phases that takes into account GVD, the peak intensity of the beat-wave can be engineered to be located at the center of the amplified pulse envelope when leaving the plasma, thereby producing an output pulse with the same total fluence, but with a peak intensity higher than would be possible using SFBRA.

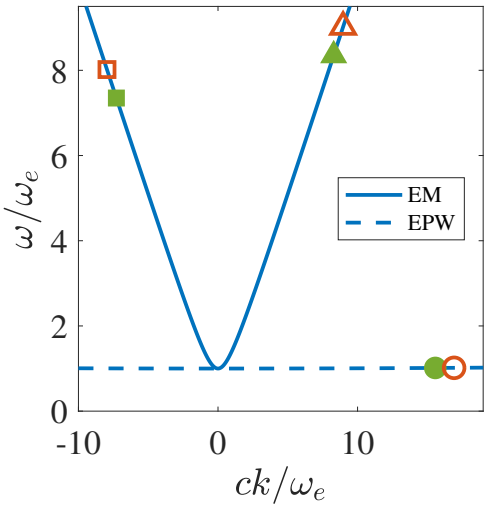

Figure 3. (Taken from Ref. [15]). Illustration of the doubly three-wave interaction in $(\omega - k)$ space. The frequencies and wave numbers of the pumps (triangles), the seeds (squares), and the EPW obey the resonance conditions of Eqs. (14) and (18) for both indices, 1 (filled points) and 2 (empty points). The solid and dashed lines are the dispersion curves of the EM wave and the EPW, respectively.

3.1. Two-frequency BRA

The idea is to launch a pump pulse and a counter-propagating seed pulse, each of them comprises two carrier frequencies, $\omega_{a_{1,2}}$ and $\omega_{b_{1,2}}$, respectively. Both frequencies obey the Raman three-wave resonant condition

$$\omega_{b_i} = \omega_{a_i} - \omega_e, \qquad i = 1, 2. \tag{14}$$

To be specific, the pump wave vector is given by

$$\mathbf{a}(t, x) = a_0 \, \Re \left[e^{i(\omega_{a_1} t + k_{a_1} x)} + e^{i(\omega_{a_2} t + k_{a_2} x)} \right] \hat{y} \tag{15}$$

and the counter-propagating seed wave vector at the plasma edge, $x = 0$ reads

$$\mathbf{b}(t, x = 0) = b_0 \, e^{-\frac{(t-t_0)^2}{2\sigma^2}} \, \Re \left[e^{i\omega_{b_1} t} + e^{i\omega_{b_2} t + i\phi)} \right] \hat{y}, \tag{16}$$

where, σ is the seed width, ϕ is the relative phase between the spectral components, and $\Re$ stands for the real part. The double resonance condition (14) implies that the spacing between the carrier frequencies is the same for the pump and the seed,

$$\delta = \omega_{a_2} - \omega_{a_1} = \omega_{b_2} - \omega_{b_1}. \tag{17}$$

For cold plasmas, the excited EPW frequencies are $\omega_{f_i} \approx \omega_e$ and the spacial resonant conditions are automatically fulfilled for both carrier frequencies,

$$k_{f_i} = k_{a_i} + k_{b_i}, \qquad i = 1, 2. \tag{18}$$

In Fig. 3 we illustrate the doubly three-wave interaction resonance conditions according to both spectral [Eq. (14)] and spacial [Eq. (18)] resonance conditions.

There are two necessary conditions for the amplification of the doubly BRA in the linear regime. The first condition ensures that the initial seed is wide enough to contain the beat

waveform, i.e., there is at least one beat oscillation inside the seed envelope. Since the temporal spacing between beat spikes depends on the spectral spacing, this condition can be written as

$$\delta > \frac{4\pi}{\sigma}. \tag{19}$$

The second condition has to do with avoiding resonant overlap between neighboring resonances. Note that this condition is analogous to the Chirikov criterion for resonance overlap in nonlinear oscillators [16]. Such an overlap mixes two or more resonances and chaotically transfers energy between modes. This interaction between spectral components is harmful to the MFBRA that is based on a coherent resonant amplification of each spectral component in the seed. The resonant width of each spectral component, determined via the linearized three-wave interaction, is equal to 2Γ, where, for linear polarization, the linear Raman growth rate is given by

$$\Gamma = \frac{a_0\sqrt{\omega_{a_1}\omega_e}}{2} \tag{20}$$

for both pump frequency because $\omega_{a_2} \approx \omega_{a_1}$. Therefore, to avoid overlap between neighboring resonances, the spectral separation, δ, must be larger than twice the resonant width, i.e.,

$$\delta > 4\Gamma. \tag{21}$$

3.2. PIC simulations

The discussion in the previous subsection was restricted to the three-wave interaction fluid model that is based on the envelope approximation and neglects kinetic effects. To show that MFBRA is applicable in a more realistic model, we employ the particle-in-cell (PIC) code EPOCH [17]. We consider a uniform unperturbed electron density of $n_0 = 2.5 \times 10^{19}\mathrm{cm}^{-3}$, electron temperature of $T_e = 30\mathrm{eV}$, and immobile ions. To reduce the simulation time, we employ a window of 0.3mm in width, moving with the seed. In order to compare SFBRA and MFBRA, we present here two simulations. One is a typical SFBRA [Fig. 4] and the second is the simplest MFBRA with just two carrier frequencies [Fig. 5].

In the first example, the (single frequency) pump wavelength is $\lambda_0 = 800\mathrm{nm}$, i.e., $\omega_0 = 2\pi \times 375$ THz and the plasma is underdense with $n_0 = 0.0145\, n_{\mathrm{cr}}$. The pump intensity is $I_0 = 10^{14}\mathrm{W/cm}^2$ so the pump dimensionless amplitude, $a_0 = 8.5 \times 10^{-10}\, \lambda_0[\mu m](I_0[\mathrm{W/cm}^2])^{0.5}$ (for linear polarization) is $a_0 = 0.068$. The seed has a Gaussian profile with a full-width half-maximum of 80 fs and its frequency was downshifted by the plasma frequency.

For the second example (MFBRA) we choose two carrier frequencies and present the PIC simulation results in Fig. 5. The frequency spacing is δ, i.e., $\omega_{a_1} = \omega_0$ and $\omega_{a_2} = \omega_0 + \delta$, such that the beat frequency is $\Omega = \delta/2 \ll \omega_0$. The total pump fluence (energy per cross area) is kept to be the same as in the single frequency example, but now, it is equally split over the two frequencies, $I_{a_1} = I_{a_2} = I_0/2 = 5 \times 10^{13}\,\mathrm{W/cm}^2$ so the dimensionless amplitudes are $a_1 = a_2 = a_0/\sqrt{2} = 0.0048$. Similarly, the seed also comprises two carrier frequencies with spacing $\delta = \omega_{b_2} - \omega_{b_1}$. To keep the total seed fluence as in the previous example, we choose $\bar{b}_0 = a_0/\sqrt{2} = 0.0048$. Usefully, we can control the location of the local spikes within the beat envelope by changing the relative phase, ϕ. Moreover, by choosing the initial phase difference, ϕ, we can compensate for the relative phase between the spectral components that is accumulated due to GVD while the seed travels through the plasma. We apply this method to the example presented in Fig. 5 where, by choosing $\phi = \pi$, we manipulate the peak intensity to be at the center of the amplified seed envelope at the end of the plasma ($x = 5.8\,\mathrm{mm}$). This optimizes the overall peak intensity in this example. Importantly, we can conclude that these two resonances remain well separated and the resonance overlap is insignificant also in the nonlinear regime when the linear estimation for the resonance width, Γ [Eq. (20)], is invalid.

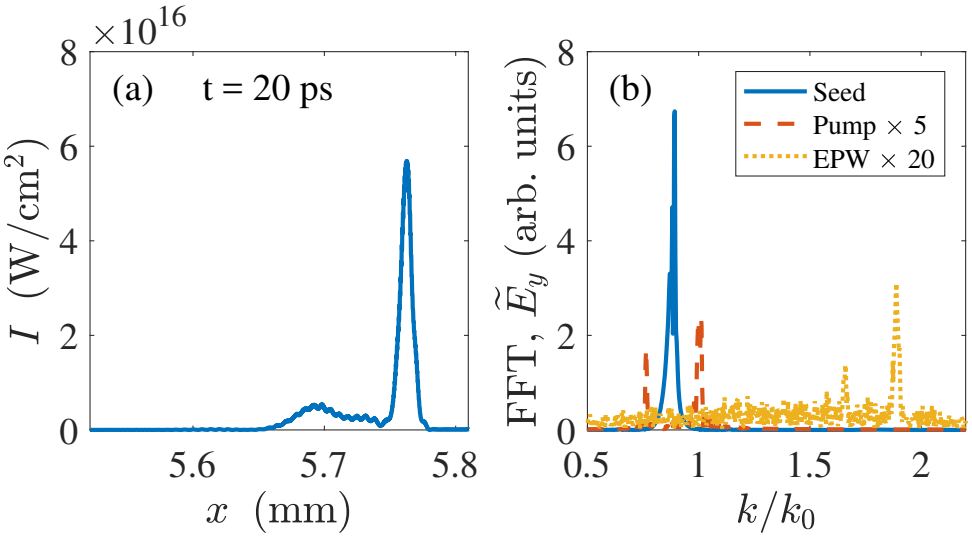

Figure 4. (Taken from [15]). PIC simulation of a SFBRA. The intensity of the amplified pulse (a) is in the nonlinear regime. The spectra (b) of the amplified seed (blue), pump (dashed red) and EPW (dotted yellow) obey the Raman resonance condition, $k_f = k_a + k_b$, where $k_a = k_0$, $k_b = 0.89k_0$, and $k_f = 1.89k_0$. A secondary Raman backscattering of the seed is also observed as smaller spikes at $k = 0.76k_0$ in the pump spectrum and $k = 1.65k_0$ in the EPW spectrum. Some backscattering of the seed is not unexpected, since the seed reaches an intensity far greater, in fact, than the pump intensity.

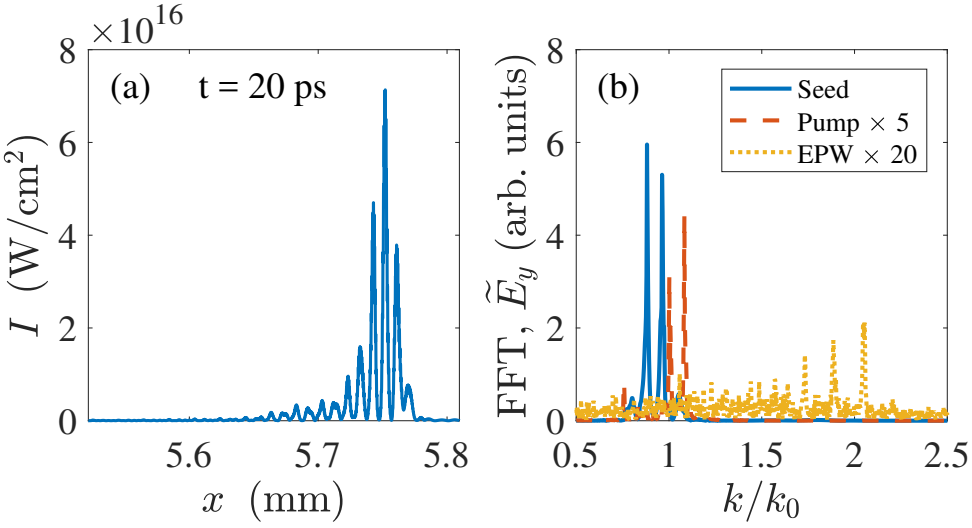

Figure 5. (Taken from [15]) . PIC simulation of a DFBRA. The intensity of the amplified pulse (a) is in the nonlinear regime with beat-wave structure. The spectra (b) of the amplified seed (blue), pump (dashed red) and EPW (dotted yellow) obey the doubly Raman resonance condition (18).

The advantages of amplifying multifrequency pulses are as follows. First, similar to other spectral approaches, such pulses experience a reduced premature reflectivity of the pump due to a smaller linear growth rate of each spectral component. However, uniquely to MFBRA, the secondary backscattering of the amplified seed is also reduced since the seed also comprises

multiple carrier frequencies. Therefore, the total (unwanted) reflectivity is reduced, and the amplification efficiency increases. Second, the duration of each spike in the beat-wave envelope is smaller than that of the envelope, and thus, one can get a much shorter pulse without additional compression. Third, by engineering the initial phases of the seed components, the maximum intensity can be optimized for the same efficiency. Additionally, following the recent study that found that the total critical intensity for self-focusing might be higher for multicolor beams [18], we expect to find a similar delay in the transverse filamentation instability since the same nonlinear Kerr term is responsible for both effects. Such a delay might enable longer amplification before encountering this transverse instability, making MFBRA even more favorable over SFBRA.

Finally, we note that it is possible to amplify pulses with more than two carrier frequencies. An example with three frequencies is presented in Ref. [6].

4. Summary

In summary, we have reviewed two spectral effects of Raman amplifiers. We showed how pump detuning can mitigate the nonlinear saturation of the leading spike. This phase mismatch mitigation provides a new tool for enhancing the amplification and reshaping the pulse waveform in the nonlinear regime when the quiver motion of the electrons in the extremely high electric field of the amplified laser become relativistic. We also found that multifrequency pulses can be Raman amplified much similar to single-frequency pulses. This provides a new tool for shorter spikes with higher peaks. Advantageously, such multifrequency pulses enjoy from noise suppression and reduced transverse instabilities.

Nevertheless, we must note that there are no free meals and both methods require a bandwidth. Future work may include kinetic and 3D effects in both regimes as well as using these tools for Brillouin amplifiers that may be advantageous in some regimes [4].

Acknowledgments

This work was supported by NNSA Grant No. DE-NA0002948 and AFOSR Grant No. FA9550-15-1-0391.

References

[1] V. M. Malkin, G. Shvets, and N. J. Fisch, Phys. Rev. Lett. **82**, 4448 (1999).
[2] G. Lehmann and K. Spatschek, Phys. Plasmas **20**, 073112 (2013).
[3] S. Weber, C. Riconda, L. Lancia, J.-R. Marque‘s, G. A. Mourou, and J. Fuchs, Phys. Rev. Lett. **111**, 055004 (2013).
[4] M. R. Edwards, Q. Jia, J. M. Mikhailova, and N. J. Fisch, Phys. Plasmas **23**, 083122 (2016).
[5] K. Qu, I. Barth, and N. J. Fisch, Phys. Rev. Lett. **118**, 164801 (2017).
[6] I. Barth, Z. Toroker, A. A. Balakin, and N. J. Fisch, Phys. Rev. E **93**, 063210 (2016).
[7] V. M. Malkin and N. J. Fisch, Eur. Phys. J. Special Topics **223**, 1157 (2014).
[8] V. M. Malkin, Z. Toroker, and N. J. Fisch, Phys. Plasmas **21**, 093112 (2014).
[9] V. M. Malkin, Z. Toroker, and N. J. Fisch, Phys. Rev. E **90**, 063110 (2014).
[10] V. M. Malkin, G. Shvets, and N. J. Fisch, Phys. Rev. Lett. **84**, 1208 (2000).
[11] I. Barth and N. J. Fisch, Phys. Plasmas **23**, 102106 (2016).
[12] V. M. Malkin, G. Shvets, and N. J. Fisch, Phys. Rev. Lett. **84**, 1208 (2000).
[13] A. A. Balakin, G. M. Fraiman, N. J. Fisch, and V. M. Malkin, Phys. Plasmas **10**, 4856 (2003).
[14] M. R. Edwards, K. Qu, J. M. Mikhailova, and N. J. Fisch, Phys. Plasmas **24**, 103110 (2017).
[15] I. Barth and N. J. Fisch, Phys. Rev, E **97**, 033201 (2018).
[16] B. V. Chirikov, Phys. Rep. **52**, 263 (1979).
[17] T. D. Arber, K. Bennett, C. S. Brady, A. Lawrence-Douglas, M. G. Ramsay, N. J. Sircombe, P. Gillies, R. G. Evans, H. Schmitz, A. R. Bell, and C. P. Ridgers, Plasma Phys. Controlled Fusion **57**, 113001 (2015).
[18] A. Sukhinin, A. B. Aceves, J. C. Diels, and L. Arissian, Phys. Rev. A **95**, 031801(R) (2017).
[19] V. M. Malkin and N. J. Fisch, Phys. Rev. Lett. **117**, 133901 (2016).